J Appl Electrochem (2010) 40:2107–2115
DOI 10.1007/s10800-010-0192-9

ORIGINAL PAPER

Inhibition effect of methyl violet on the corrosion of cold rolled steel in 1.0 M sulfuric acid solution

Shu-Duan Deng · Xiang-Hong Li · Hui Fu

Received: 29 January 2010 / Accepted: 5 September 2010 / Published online: 18 September 2010

Abstract The inhibition effect of methyl violet (MV) on the corrosion of cold rolled steel (CRS) in 1.0 M sulfuric acid (H_2SO_4) was investigated by weight loss, potentiodynamic polarization, and electrochemical impedance spectroscopy (EIS) methods. The results show that MV is a good inhibitor, and inhibition efficiency increases with inhibitor concentration, while decreases with the temperature. The adsorption of MV on CRS surface obeys Langmuir adsorption isotherm equation. The thermodynamic parameters of adsorption enthalpy ($\Delta H°$), adsorption free energy ($\Delta G°$) and adsorption entropy ($\Delta S°$) are calculated and discussed. Potentiodynamic polarization curves show that MV acts as a mixed-type inhibitor in sulfuric acid. EIS exhibits one capacitive loop which indicates that the corrosion reaction is controlled by charge transfer process. Inhibition efficiency values obtained from weight loss, polarization and EIS are in reasonably good agreement. The adsorbed film on CRS surface containing optimum dose of MV was investigated by Fourier transform infrared spectroscopy (FTIR) and scanning electron microscopy (SEM). Depending on the results, the inhibitive mechanism is proposed from the viewpoint of adsorption theory.

Keywords Methyl violet · Corrosion inhibitor · Adsorption · Sulfuric acid · Cold rolled steel · Weight loss · Polarization · EIS · FTIR · SEM

S.-D. Deng (✉)
Faculty of Wood Science and Decoration Technology, Southwest Forestry University, Kunming 650224, People's Republic of China
e-mail: dengshuduan@163.com

X.-H. Li · H. Fu
Department of Fundamental Courses, Southwest Forestry University, Kunming 650224, People's Republic of China

1 Introduction

The use of inhibitors is one of the most practical methods for protection metals against corrosion, especially in acidic media [1]. Most well-known acid inhibitors are organic compounds containing polar functions with nitrogen, sulfur, or oxygen atoms as well as those with triple or conjugated double bonds or aromatic rings in their molecular structures. It is generally accepted that organic molecules inhibit corrosion by adsorption on the metal surface and that the adsorption depends on the molecule's chemical composition, temperature and electrochemical potential at the metal/solution interface. So the study of the relationship between adsorption and corrosion inhibition is of great importance.

Among various organic inhibitors, organic dyes whose molecules meet certain desirable characteristics as potential corrosion inhibitors have been attracted more attention. For example, Tang et al. studied the inhibition of steel corrosion in 1.0 M HCl by neutral red (NR) [2] and 1-(2-pyridylazo)-2-naphthol (PAN) [3]. Afterwards, Oguzie et al. investigated a series of dyes as good corrosion inhibitors for mild steel in HCl and H_2SO_4 media, such as indigo dye [4], thymol blue [5], congo red [6], methylene blue [7, 8] and crystal violet [9]. Recently, Abboud et al. [10] reported that the inhibition efficiency of a synthesized dye of 8-quinolinol-5-azoantipyrine (HQAP) on mild steel in 1.0 M HCl is higher than 90% at 0.1 mM. In addition, some traditional analytical indicators, e.g. methyl red [11] and cresol red [12] also behave as good inhibitors for steel in acid media. However, data about the use of organic dyes as corrosion inhibitors are scarce. Further studies are still essential. Methyl violet (MV) is an ordinary analytical indicator with low-cost and easy production. Up to now, literature about using MV as corrosion inhibitor for steel in acid solution is almost scant.

In order to extend organic dyes as inhibitors, this paper focuses on the corrosion inhibition by MV for cold rolled steel (CRS) in 1.0 M H_2SO_4. Weight loss, potentiodynamic polarization curves, and electrochemical impedance spectroscopy (EIS) methods were employed to evaluate corrosion rate and inhibition efficiency. Meanwhile, the steel surface was examined by scanning electron microscope (SEM). Moreover, the adsorption isotherm of MV on CRS surface is obtained. The thermodynamic parameters (adsorption enthalpy $\Delta H°$, adsorption free energy $\Delta G°$ and adsorption entropy $\Delta S°$) are calculated and discussed in detail. It is expected to provide useful information on the adsorption and inhibition effect of MV on steel in sulfuric acid solution.

2 Experimental method

2.1 Materials

Tests were performed on a CRS of the following composition (wt%): 0.07% C, 0.3% Mn, 0.022% P, 0.010% S, 0.01% Si, 0.030% Al, and bal. Fe.

2.2 Inhibitor

The organic dye of methyl violet (MV) was obtained from Shanghai Chemical Reagent Company of China. Figure 1 shows its molecular structure.

2.3 Solutions

The aggressive solutions, 1.0 M H_2SO_4 were prepared by dilution of analytical grade 98% H_2SO_4 with distilled water. The concentration range of MV used is 0.02–0.20 mM (2.0×10^{-5}–2.0×10^{-4} M).

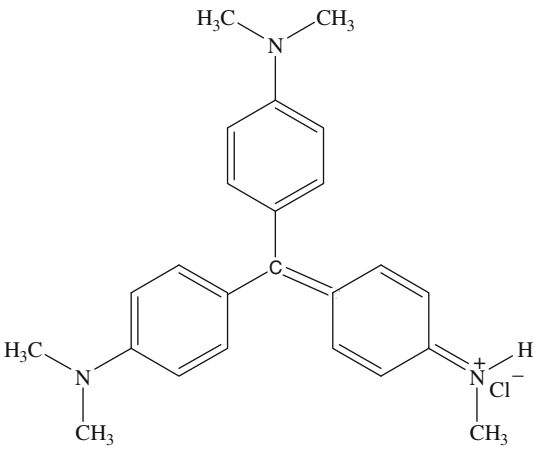

Fig. 1 Chemical molecular structure of methyl violet (MV)

2.4 Weight loss measurements

The CRS sheets of 2.5 cm × 2.0 cm × 0.06 cm were abraded with a series of emery paper (grade 320-500-800) and then washed with distilled water and acetone. After weighing accurately by electronbalance (± 0.1 mg), three parallel specimens were immersed in a beaker containing 250 mL 1.0 M H_2SO_4 solution without and with different concentrations of MV. All the aggressive acid solutions were open to air. After 6 h the specimens were taken out, washed, dried, and weighed accurately. The average weight loss of three parallel CRS sheets was obtained. Then the tests were repeated at different temperatures using a water thermostat (±0.1 °C). The corrosion rate (v) was calculated by the following equation [13]:

$$v = \frac{W}{St} \tag{1}$$

where W is the average weight loss of three parallel CRS sheets, S the total area of one CRS specimen and t is immersion time. With the calculated corrosion rate, inhibition efficiency obtained from weight loss (E_w) was calculated by [13]:

$$E_w\,(\%) = \frac{v_0 - v}{v_0} \times 100 \tag{2}$$

where v_0 and v are the values of the corrosion rate without and with the inhibitor, respectively.

2.5 Electrochemical measurements

Electrochemical experiments were carried out in the conventional three-electrode cell with a platinum counter electrode (CE) and a saturated calomel electrode (SCE) coupled to a fine Luggin capillary as the reference electrode. In order to minimize ohmic contribution, the Luggin capillary was close to working electrode (WE). WE was in the form of a square CRS embedded in PVC holder using epoxy resin so that the flat surface was the only surface in the electrode. The working surface area was 1.0 cm × 1.0 cm, abraded with emery paper (grade 320-500-800) on test face, rinsed with distilled water, degreased with acetone, and dried with a cold air stream. Before measurement the electrode was immersed in test solution at open circuit potential (OCP) for 2 h to be sufficient to attain a stable state. All electrochemical measurements were carried out using PARSTAT 2273 advanced electrochemical system (Princeton Applied Research). Each experiment was repeated at least three times to check the reproducibility.

The potential of potentiodynamic polarization curves increased at 0.5 mV s^{-1} and started from a potential of

−250 to +250 mV versus free corrosion potential (E_{corr} vs. SCE). Inhibition efficiency (E_p, %) is defined as:

$$E_p\ (\%) = \frac{I_{corr} - I_{corr(inh)}}{I_{corr}} \times 100 \quad (3)$$

where I_{corr} and $I_{corr(inh)}$ represent corrosion current density values without and with inhibitor, respectively.

Electrochemical impedance spectroscopy (EIS) was carried out at OCP in the frequency range of 0.01 Hz–100 kHz using a 10 mV peak-to-peak voltage excitation. Inhibition efficiency (E_R, %) is determined using the equation:

$$E_R\ (\%) = \frac{R_{t(inh)} - R_{t(0)}}{R_{t(inh)}} \times 100 \quad (4)$$

where $R_{t(0)}$ and $R_{t(inh)}$ are charge transfer resistance values for CRS in the absence and presence of inhibitor, respectively.

2.6 Fourier transform infrared spectroscopy (FTIR)

FTIR spectra were recorded in an AVATAR-FTIR-360 spectrophotometer (Thermo Nicolet Company, USA).In order not to damage the adsorbed layer of the CRS surfaces after immersion in uninhibited and inhibited H_2SO_4 solutions, the FTIR reflectance accessory was applied to measure the CRS surfaces [14].

2.7 Scanning electron microscopy (SEM)

Samples of dimension 2.5 cm × 2.0 cm × 0.06 cm were prepared as described above (Sect. 2.4). After immersion in 1.0 M H_2SO_4 without and with 0.20 mM MV at 20 °C for 6 h, the specimens were thoroughly washed with distilled water, dried with a cold air blaster. SEM experiments were performed with Japan instrument model S-3000N scanning electron microscope (Hitachi High-Tech Science Systems Corporation).

3 Experimental results and discussion

3.1 Weight loss measurements

3.1.1 Effect of MV on corrosion rate

Figure 2 shows the corrosion rate values of CRS with different concentrations of MV in 1.0 M H_2SO_4 solution at 20–50 °C. The corrosion rate decreases as the concentration of MV increases, i.e. the corrosion inhibition enhances with the inhibitor concentration. This behavior is due to the fact that the adsorption coverage of inhibitor on CRS surface increases with the inhibitor concentration [14].

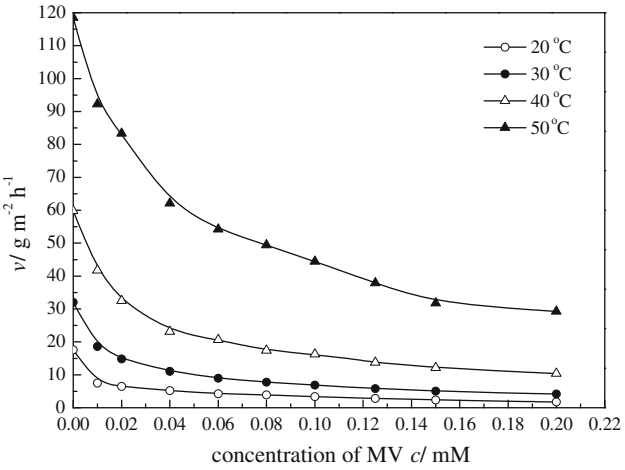

Fig. 2 Relationship between corrosion rate (v) and concentration of MV (c) in 1.0 M H_2SO_4

It should be noted that the corrosion rate reaches certain value within the studied temperature range at about 0.15 mM MV. Also, it increases with temperature both in uninhibited and inhibited solutions, especially more rapidly in the absence of inhibitor. These results confirm that MV acts as an efficient inhibitor in the range of temperature studied.

3.1.2 Effect of MV on inhibition efficiency

Values of inhibition efficiency obtained from the weight loss (E_w) for different inhibitor concentrations in 1.0 M H_2SO_4 are shown in Fig. 3. E_w increases in the concentration range of inhibitor from 0.02 to 0.20 mM, and the maximum E_w is 90.2% at 20 °C, which indicates that MV is a good inhibitor for CRS in 1.0 M H_2SO_4.

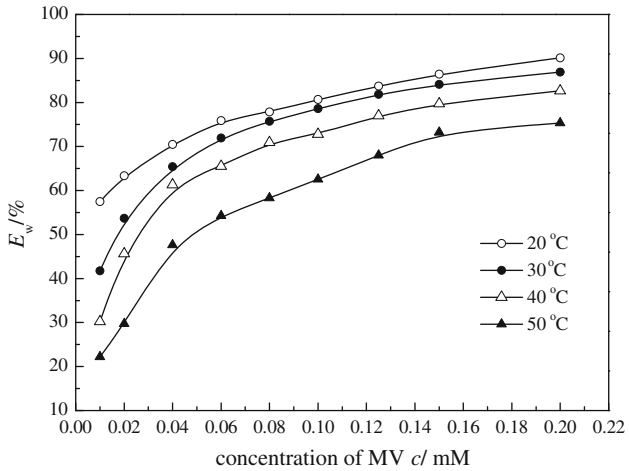

Fig. 3 Relationship between inhibition efficiency (E_w) and concentration of MV (c) in 1.0 M H_2SO_4

Further inspection of Fig. 3 reveals that the E_w decreases with temperature, which could be ascribed to that higher temperatures cause desorption of the inhibitor.

3.1.3 Adsorption isotherm

Basic information on the interaction between inhibitor and steel surface can be provided by the adsorption isotherm. Attempts were made to fit to various isotherms including Frumkin, Langmuir, Temkin, Freundlich, Bockris–Swinkels and Flory–Huggins isotherms. By far the results are best fitted by Langmuir adsorption isotherm [15]:

$$\frac{c}{\theta} = \frac{1}{K} + c \tag{5}$$

where c is the concentration of inhibitor, K the adsorptive equilibrium constant and θ is the surface coverage which can be calculated by the following equation [15]:

$$\theta = \frac{v_0 - v}{v_0} \tag{6}$$

From the values of surface coverage, the linear regressions between c/θ and c are calculated, and the parameters are listed in Table 1. Figure 4 shows the relationship between c/θ and c at 20–50 °C. Clearly, all linear correlation coefficients (r) almost equal to 1, and slope values are close to 1, which indicates the adsorption of MV on steel surface obeys the Langmuir adsorption isotherm. Noticeably, the slope of the straight line is slightly different from 1, which could be attributed to that there is a interaction force in the adsorption layer [16].

The adsorptive equilibrium constant (K) value decreases with increase in temperature. Generally, large value of K means better inhibition performance of a given inhibitor. This result agrees well with the values of E_w obtained from Fig. 3.

3.1.4 Thermodynamic parameters

Thermodynamic parameters play an important role in understanding inhibitive mechanism. The adsorption enthalpy (ΔH) was calculated according to the Van't Hoff equation [13–15]:

$$\ln K = \frac{-\Delta H}{RT} + \text{constant} \tag{7}$$

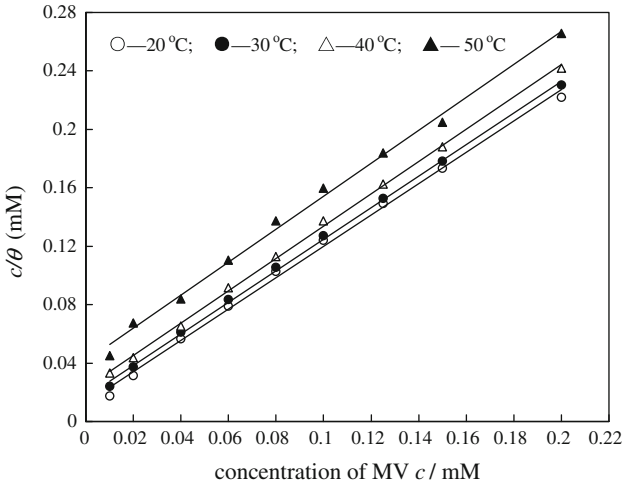

Fig. 4 The relationship between c/θ and c in 1.0 M H_2SO_4. (*Open circle*) 20 °C; (*filled circle*) 30 °C; (*open triangle*) 40 °C; (*filled triangle*) 50 °C

where R is the gas constant (8.314 J K^{-1} mol^{-1}), T the absolute temperature (K).

According to Eq. 7, $-\Delta H/R$ is the slope of straight line of ln K versus $1/T$ shown in Fig. 5. Under the experimental conditions, ΔH can be approximately regarded as the standard adsorption enthalpy ($\Delta H°$) [13–15].

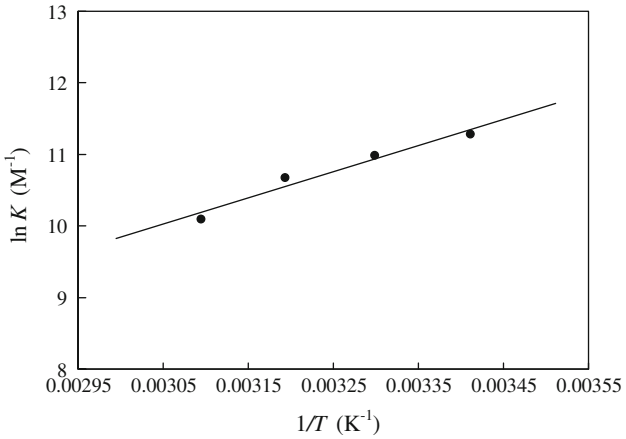

Fig. 5 The relationship between ln K and $1/T$

Table 1 Parameters of the linear regression between c/θ and c in 1.0 M H_2SO_4

Temperature (°C)	Linear correlation coefficient (r)	Slope	Intercept (mM)	K (M^{-1})
20	0.9963	1.07	0.0126	7.91×10^4
30	0.9988	1.08	0.0170	5.90×10^4
40	0.9990	1.11	0.0232	4.31×10^4
50	0.9950	1.13	0.0414	2.42×10^4

The adsorptive equilibrium constant (K) is related to the standard adsorption free energy (ΔG°) obtained according to [17]:

$$K = \frac{1}{55.5}\exp\left(\frac{-\Delta G^\circ}{RT}\right) \quad (8)$$

where the value 55.5 is the concentration of water in solution expressed in M [17]. Then the standard adsorption entropy (ΔS°) can be obtained by the following basic thermodynamic equation:

$$\Delta S^\circ = \frac{\Delta H^\circ - \Delta G^\circ}{T} \quad (9)$$

All the calculated thermodynamic parameters are listed in Table 2. The negative value of ΔH° shows that the adsorption of inhibitor is an exothermic process [14], which indicates that inhibition efficiency decreases with increase in temperature. Such behavior can be interpreted on the basis that the increase in temperature resulted in desorption of some adsorbed inhibitor molecules from the metal surface. The negative value of ΔG° suggests that the adsorption of inhibitor molecule onto steel surface is a spontaneous process. Generally, values of ΔG° up to -20 kJ mol^{-1} are consistent with the electrostatic interaction between the charged molecules and the charged metal (physical adsorption) while those more negative than -40 kJ mol^{-1} involve sharing or transfer of electrons from the inhibitor molecules to the metal surface to form a co-ordinate type of bond (chemisorption) [17, 18]. In the present study, the value of ΔG° ranging from -20 to -40 kJ mol^{-1} means that the adsorption of MV on CRS surface involves both physical adsorption and chemical adsorption.

Interestingly, the sign of ΔS° is positive. This is opposite to what would be expected, since adsorption is an exothermic process always accompanied by a decrease of entropy. The reason could be explained as follows: The adsorption of organic inhibitor molecules from the aqueous solution can be regarded as a quasi-substitution process between the organic compound in the aqueous phase [$Org_{(sol)}$] and water molecules at the electrode surface [$H_2O_{(ads)}$] [19]. In this situation, the adsorption of organic inhibitor is accompanied by desorption of water molecules from the surface. Thus, while the adsorption process for the inhibitor is believed to be exothermic and associated with a decrease in entropy of the solute, the opposite is true for the solvent. The thermodynamic values obtained are the algebraic sum of the adsorption of organic molecules and the desorption of water molecules [20]. Therefore, the gain in entropy is attributed to the increase in solvent entropy [20]. The positive values of ΔS° mean that the adsorption process is accompanied by an increase in entropy, which is the driving force for the adsorption of inhibitor onto the CRS surface [19].

Table 2 Thermodynamic parameters of the adsorption of MV on CRS surface in 1.0 M H_2SO_4

Temperature (°C)	ΔG° (kJ mol^{-1})	ΔH° (kJ mol^{-1})	ΔS° (J mol^{-1} K^{-1})
20	−37.28	−30.34	20.02
30	−37.81	−30.34	24.64
40	−38.24	−30.34	25.55
50	−37.91	−30.34	23.43

3.2 Polarization studies

Figures 6 and 7 show the potentiodynamic polarization curves for CRS in 1.0 M H_2SO_4 solution containing

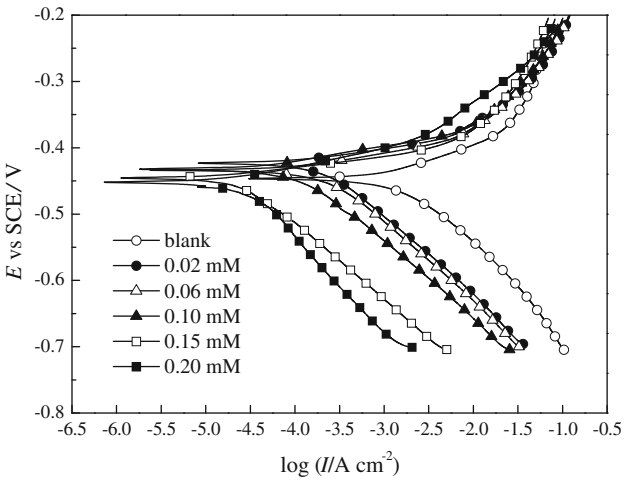

Fig. 6 Potentiodynamic polarization curves for CRS in 1.0 M H_2SO_4 containing MV at 20 °C

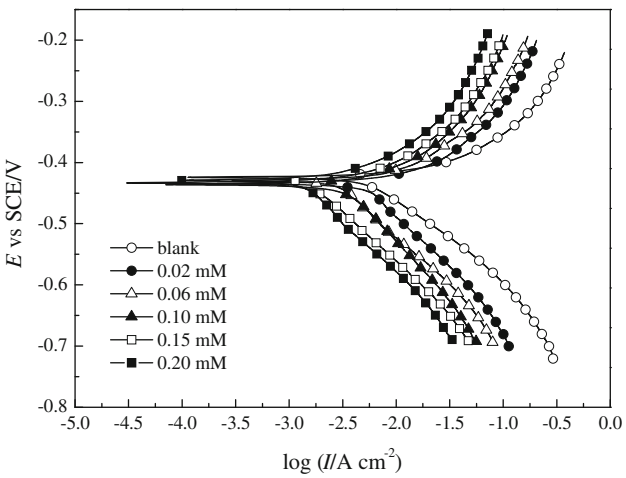

Fig. 7 Potentiodynamic polarization curves for CRS in 1.0 M H_2SO_4 containing MV at 50 °C

Table 3 Potentiodynamic polarization parameters for the corrosion of CRS in 1.0 M H_2SO_4 containing different concentration of MV at 20 and 50 °C

Temperature (°C)	c (mM)	E_{corr} vs. SCE (mV)	I_{corr} (μA cm^{-2})	b_c (mV dec^{-1})	b_a (mV dec^{-1})	E_p (%)
20	0	−447.0	816.7	122	66	–
	0.02	−433.5	299.5	110	32	63.3
	0.06	−432.2	221.8	103	32	72.8
	0.10	−423.2	167.3	108	27	79.5
	0.15	−449.6	113.8	117	32	86.1
	0.20	−445.2	72.0	111	21	91.2
50	0	−433.9	4649.0	146	60	–
	0.02	−437.5	3041.4	184	48	34.6
	0.06	−441.0	2084.1	165	54	55.2
	0.10	−441.6	1651.3	198	74	64.5
	0.15	−440.0	1101.8	184	55	76.3
	0.20	−441.7	898.2	179	65	80.7

various concentrations of MV at 20 and 50 °C, respectively. At both temperatures, the presence of MV causes a remarkable decrease in the corrosion rate i.e., shifts the both anodic and cathodic curves to lower current densities, while the cathodic decrease is more significant. The corrosion parameters including corrosion current densities (I_{corr}), corrosion potential (E_{corr}), cathodic Tafel slope (b_c), anodic Tafel slope (b_a), and inhibition efficiency (E_p) are listed in Table 3.

Table 3 shows that I_{corr} decreases while E_p increases with the inhibitor concentration. E_p of 0.20 mM MV reaches up to a maximum of 91.2% at 20 °C; and 80.7% at 50 °C. The presence of MV does not prominently shift the corrosion potential, which indicates MV acts as a mixed-type inhibitor [21]. Tafel slopes of b_c and b_a change upon addition of MV, which implies that the MV molecules are adsorbed on both anodic and cathodic sites resulting in an inhibition of both anodic dissolution and cathodic reduction reactions. In general, MV acts as a mixed-type inhibitor while prominently retards the cathodic reaction at 20 and 50 °C.

3.3 Electrochemical impedance spectroscopy (EIS)

Figures 8 and 9 show the Nyquist diagrams for CRS in 1.0 M H_2SO_4 at 20 and 50 °C containing various concentrations of MV, respectively. At either low temperature (20 °C) or high temperature (50 °C), the impedance spectra exhibit one single depressed semicircle, and the diameter of semicircle increases with the increase of inhibitor concentration. The single semicircle indicates that the charge transfer takes place at electrode/solution interface, and the corrosion reaction of steel is controlled by the transfer process [22]. Also, these impedance diagrams are not perfect semicircles which are related to the frequency dispersion as a result of the roughness and inhomogeneous

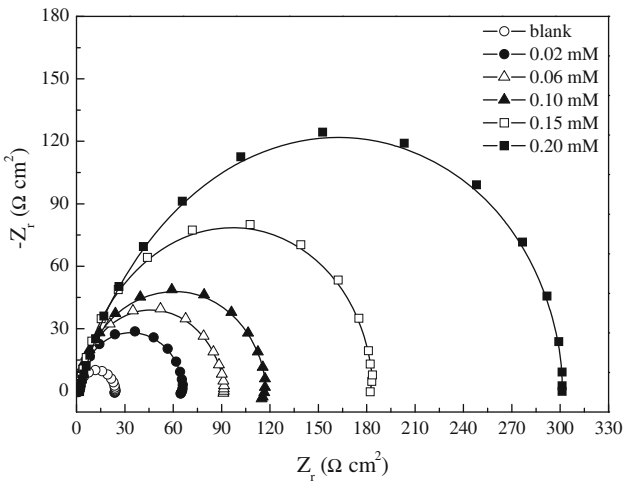

Fig. 8 EIS of the corrosion of CRS in 1.0 M H_2SO_4 with different concentrations of MV at 20 °C

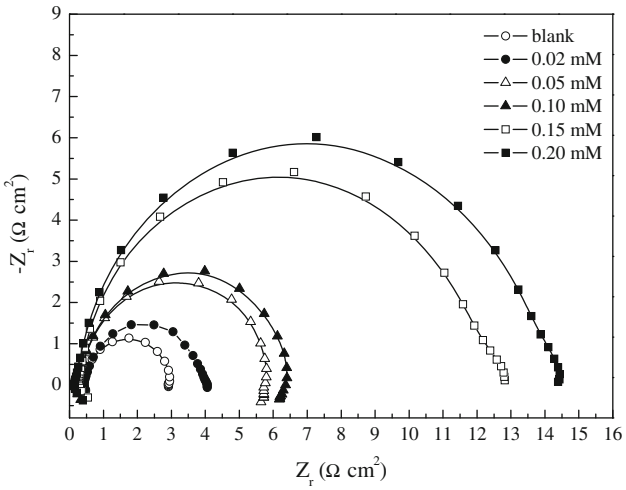

Fig. 9 EIS of the corrosion of CRS in 1.0 M H_2SO_4 with different concentrations of MV at 50 °C

of electrode surface [23]. Furthermore, the impedance response of CRS in uninhibited H_2SO_4 solution has changed significantly after addition of MV in the corrosive solution; as a result, real axis intercept at high and low frequencies in the presence of inhibitor is bigger than that in the absence of inhibitor (blank solution) and increases as the inhibitor concentration increases. This confirms that the impedance of inhibited substrate increases with the concentration of MV in 1.0 M H_2SO_4.

The EIS results are simulated by the equivalent circuit shown in Fig. 10 to pure electric models that could verify or rule out mechanistic models and enable the calculation of numerical values corresponding to the physical and/or chemical properties of the electrochemical system under investigation [24]. The circuit employed allows the identification of both solution resistance (R_s) and charge transfer resistance (R_t). It should be noted that, the double layer capacitance (C_{dl}) value is affected by imperfections of the surface, and this effect is simulated via a constant phase element (CPE) [25]. The CPE is composed of a component Q_{dl} and a coefficient *a*. The parameter *a* quantifies different physical phenomena like surface inhomogeneousness resulting from surface roughness, inhibitor adsorption, porous layer formation, etc. Therefore, the capacitance C_{dl} is deduced from the following relation [26]:

$$C_{dl} = Q_{dl} \times (2\pi f_{max})^{a-1} \quad (10)$$

where f_{max} represents the frequency at which imaginary value reaches a maximum on the Nyquist plot. The electrochemical parameters of R_t, C_{dl} and E_R are calculated by ZSimpWin software and presented in Table 4.

Inspection of Table 4 reveals that R_t values increases prominently while C_{dl} reduces with the concentration of MV. The greatest effect was observed at 0.20 mM of MV which gives R_t value of 307.7 Ω cm^2 at 20 °C, and 14.1 Ω cm^2 at 50 °C; C_{dl} value of 74.4 μF cm^{-2} at 20 °C, and 371.4 μF cm^{-2} at 50 °C. The decrease in C_{dl} comparing with that in blank solution (without inhibitor), which can result from a decrease in local dielectric constant and/or an increase in the thickness of the electrical double layer, suggests that the inhibitor molecules function by adsorption at the metal/solution interface [27]. E_R increases with MV concentration, and follows the order: E_R (20 °C) > E_R (50 °C). E_R values reach the maximum of 92.5% (20 °C) and 81.6% (50 °C), which further confirms

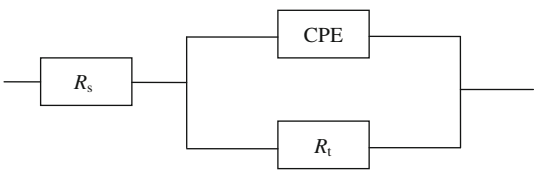

Fig. 10 The equivalent circuit model of EIS

Table 4 EIS parameters for the corrosion of CRS in 1.0 M H_2SO_4 containing MV at 20 and 50 °C

Temperature (°C)	*c* (mM)	R_t (Ω cm^2)	C_{dl} (μF cm^{-2})	E_R (%)
20	0	23.1	240.3	–
	0.02	65.0	229.7	64.5
	0.06	91.3	148.7	74.7
	0.10	117.6	115.5	80.4
	0.15	185.0	90.2	87.5
	0.20	307.7	74.4	92.5
50	0	2.6	2703.1	–
	0.02	3.7	1415.2	29.7
	0.06	5.6	935.1	53.6
	0.10	6.3	831.2	58.7
	0.15	12.3	425.7	78.9
	0.20	14.1	371.4	81.6

that MV exhibits very good inhibitive performance for CRS in 1.0 M H_2SO_4.

Inhibition efficiencies obtained from weight loss (E_w), potentiodynamic polarization curves (E_p) and EIS (E_R) are in good agreement.

3.4 Fourier transform infrared spectroscopy

FTIR spectrometer is a powerful instrument that can be used to determine the type of bonding for organic inhibitors absorbed on the metal surface [13, 14, 28]. In this article, FTIR spectrometer is used to identify whether there is adsorption and to provide new bonding information on the steel surface after immersion in inhibited H_2SO_4 solution.

The FTIR reflectance spectrum of corrosion layer formed on the CRS surface after 6 h immersion in 1.0 M H_2SO_4 is shown in Fig. 11a. The weak bands at 3827 and 3692 cm^{-1} are assigned to Fe–O bending [28], and the bands at 877, 818 and 758 cm^{-1} arise form FeOOH and Fe_2O_3 [29], which reveal the fact that the adsorbed protective film is oxidized by O_2 and H_2O in air. The band at 3363 cm^{-1} is attributed to O–H stretching, which further indicate the protective film contains H_2O. There is a peak at 1104 cm^{-1}, which is attributed to the S=O stretching of SO_4^{2-} [14]. The SO_4^{2-} in CRS corrosion layer comes from the corrosion product of $FeSO_4$.

Figure 11b shows the FTIR spectrum of adsorbed protective layer formed CRS surface after immersion in 1.0 M H_2SO_4 containing 0.20 mM MV. Fe–O bending bands are found at 3861 and 3759 cm^{-1}. The bands at 3928 and 3620 cm^{-1} which do not appear in Fig. 11a may be assigned to Fe–N bending, which reveal the fact that MV can adsorb on the metal surface on the basis of donor-acceptor interactions between lone-pair electrons of N and the vacant d-orbital of Fe substrate. It is found that the N–H stretch at

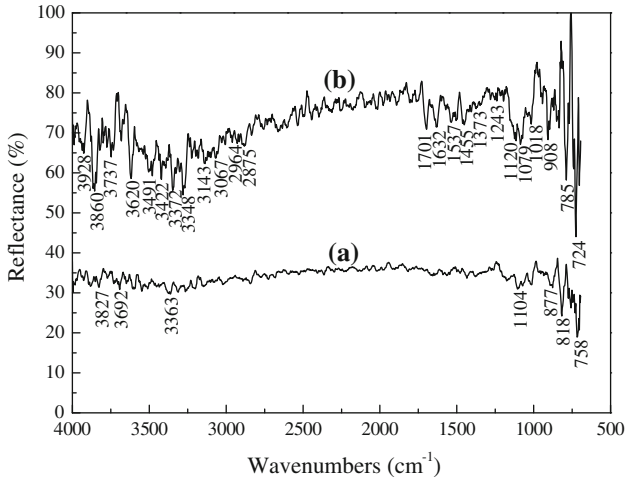

Fig. 11 FTIR spectra of adsorption layer formed on the CRS surface after immersion in various solutions (*a*) after 6 h of immersion at 20 °C in 1.0 M H_2SO_4; (*b*) after 6 h of immersion at 20 °C in 0.20 mM MV + 1.0 M H_2SO_4

3491 and 3422 cm^{-1}, and O–H stretch at 3372 and 3348 cm^{-1}. The weak bands at 3143 and 3067 cm^{-1} is attributed to C–H stretching vibration in benzene. The bands at 2964 and 2875 cm^{-1} are attributed to the aliphatic C–H asymmetric and symmetric stretching vibrations, respectively. The C=N weak stretching vibration at 1701 cm^{-1} and the C=C (or C=N) stretching vibration at 1635 cm^{-1} further confirm that formation of the MV inhibitor adsorbed on steel surface. The absorption bands at 1537, 1455 and 1243 cm^{-1} is due to the framework vibration of benzene ring. The band at 1373 cm^{-1} is attributed to $–CH_3$. Besides these, there are absorption bands at 1120 and 1079 cm^{-1}, which can be assigned to the C–N stretching vibration. The bands around or below 1000 cm^{-1} can be assigned to the C–H bending vibration in benzene. Comparing Fig. 11a and b, it can be suggested that MV is absorbed on the CRS surface.

3.5 Scanning electron microscope (SEM)

Figure 12 shows the SEM photos of CRS surface in 1.0 M H_2SO_4. Figure 12a and c reveals that the CRS surface after immersion in uninhibited 1.0 M H_2SO_4 at 20 and 50 °C shows an aggressive attack of the corroding medium on the steel surface. Moreover, the surface layer is rather rough. In contrast, in the presence of 0.20 mM MV, there is an adsorbed film adsorbed on CRS surface at 20 °C (Fig. 12b) and 50 °C (Fig. 12d), which does not exist in corresponding Fig. 12a and c. In accordance, it could be concluded that the adsorption film can efficiently inhibit the corrosion of steel. Also, when the temperature is increased, the corrosion is accelerated.

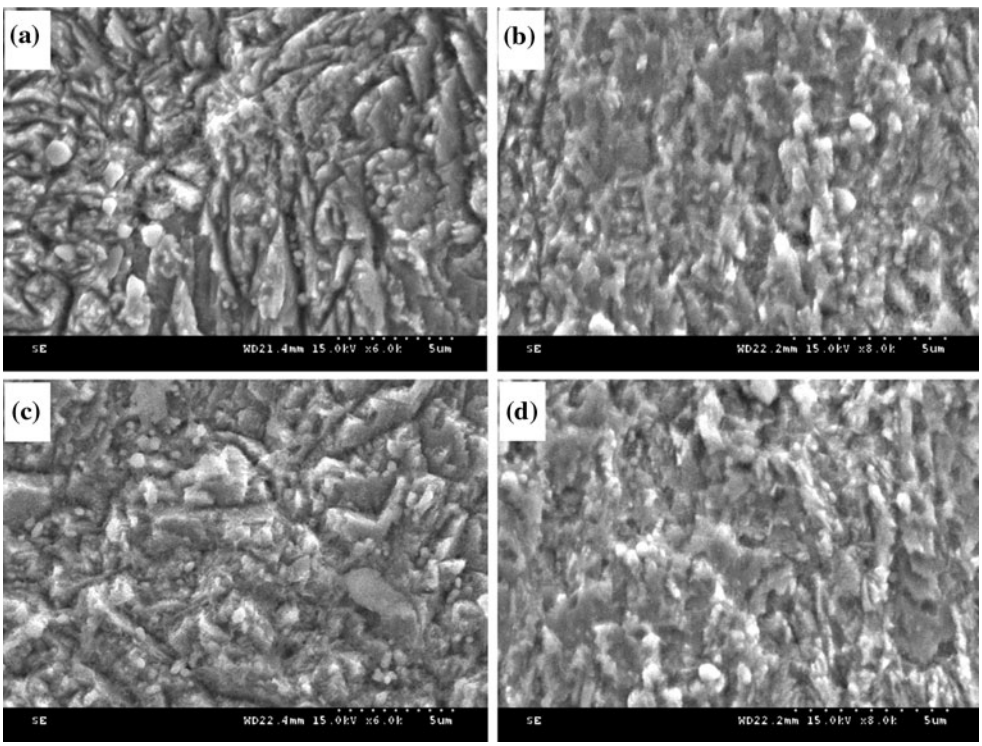

Fig. 12 SEM micrographs of CRS surface: **a** after 6 h of immersion at 20 °C in 1.0 M H_2SO_4; **b** after 6 h of immersion at 20 °C in 0.20 mM MV + 1.0 M H_2SO_4; **c** after 6 h of immersion at 50 °C in 1.0 M H_2SO_4; **d** after 6 h of immersion at 50 °C in 0.20 mM MV + 1.0 M H_2SO_4

3.6 Explanation for inhibition

MV can be classified as a 1:1 electrolyte, namely, the organic part (MV^+) is the cation and the inorganic part (Cl^-) is the anion:

$$MV \rightarrow MV^+ + Cl^- \quad (11)$$

Owing to two neutral N atoms in MV^+, MV^+ could further be protonated in the acid solution as following:

$$MV^+ + xH^+ \leftrightarrow [MVHx]^{(x+1)+} \quad (12)$$

It is well known that the steel surface charges positive charge in H_2SO_4 because of $E_{corr} - E_{q=0}$ (zero charge potential) > 0 [30], so it is difficult for MV^+ and $[MVH_x]^{(x+1)+}$ to approach the positively charged steel surface due to the electrostatic repulsion. On the other hand, Cl^- (the anion part of MV) and SO_4^{2-} could adsorb on the metal surface [31], MV^+ and $[MVH_x]^{(x+1)+}$ may adsorb on the negatively charged metal surface (physical adsorption), followed by the partial transference of electrons from the polar atom (N atom) to the d-orbital of iron atom (chemical adsorption). In other words, in the process of adsorption both physical adsorption and chemical adsorption would take place, and then the protective film is formed on the CRS surface to keep it from corrosion.

4 Conclusions

(1) Methyl violet (MV) acts as a good inhibitor for the corrosion of CRS in 1.0 M H_2SO_4, and its maximum inhibition efficiency (E) is higher than 90%. E increases with the inhibitor concentration, while decrease with the temperature.

(2) The adsorption of MV on the steel surface obeys Langmuir adsorption isotherm. The adsorption process is a spontaneous and exothermic process accompanied by an increase in entropy.

(3) MV acts as a mixed-type inhibitor in 1.0 M H_2SO_4, while prominently inhibits the cathodic reduction. EIS spectra exhibit one capacitive loop which indicates the corrosion reaction is controlled by charge transfer process. The addition of MV to 1.0 M H_2SO_4 solutions enhances R_t values while reduces C_{dl} values.

(4) FTIR and SEM results clearly show that MV inhibits corrosion of steel by being adsorbed on the metal surface.

Acknowledgments This study was carried out in the scope of research project funded by Key Laboratory for Forest Resources Conservation and Use in the Southwest Mountains of China (Southwest Forestry University) Ministry of Education, Key Construction Course of Chemical Engineering for Forest Products of Southwest Forestry University (XKX200907), and the Natural Science Foundation of Southwest Forestry University under the Grant No. 200715M. The electrochemical measurements were carried out using PARSTAT 2273 advanced electrochemical system (Princeton Applied Research) provided by Advanced Science Instrument Sharing Center of Southwest Forestry University.

References

1. Trabanelli G (1991) Corrosion 47:410
2. Tang LB, Mu GN, Liu GH (2003) Corros Sci 45:2251
3. Tang LB, Li XM, Li N, Qu Q, Mu GN, Liu GH (2005) Mater Chem Phys 94:353
4. Oguzie EE, Unaegbu C, Ogukwea CN, Okolue BN, Onuchuku AI (2004) Mater Chem Phys 84:363
5. Ebenso EE, Oguzie EE (2005) Mater Lett 59:2163
6. Oguzie EE (2004) Mater Chem Phys 87:212
7. Oguzie EE, Onuoha GN, Onuchuku AI (2005) Mater Chem Phys 89:305
8. Oguzie EE (2005) Mater Lett 59:1076
9. Oguzie EE, Njoku VO, Enenebeaku CK, Akalezi CO, Obi C (2008) Corros Sci 50:3480
10. Abboud Y, Abourriche A, Saffaj T, Berrada M, Charrouf M, Bennamara A, Hannache H (2009) Desalination 237:175
11. Liu RQ, Xiang L, Zhang XG, Xia X (2001) Corros Prot 22:98 (in Chinese)
12. Li XH, Deng SD, Fu H, Zhao N, Li YX, Mu GN (2009) Corros Sci Prot Technol 21:354 (in Chinese)
13. Li XH, Deng SD, Fu H, Mu GN (2009) J Appl Electrochem 39:1125
14. Li XH, Mu GN (2005) Appl Surf Sci 252:1254
15. Li XH, Deng SD, Fu H (2009) Corros Sci 51:1344
16. Mu GN, Li XH, Qu Q, Zhou J (2006) Corros Sci 48:445
17. Li WH, He Q, Zhang ST, Pei CL, Hou BR (2008) J Appl Electrochem 38:289
18. Bentiss F, Lebrini M, Lagrenée M (2005) Corros Sci 47:2915
19. Li XH, Deng SD, Mu GN, Fu H (2008) Corros Sci 50:2635
20. Ateya B, El-Anadauli B, Nizamy FE (1984) Corros Sci 24:509
21. Cao CN (2004) Corrosion electrochemistry mechanism. Chemical Engineering Press, Beijing, p 235 (in Chinese)
22. Larabi L, Harek Y, Traisnel M, Mansri A (2004) J Appl Electrochem 34:833
23. Lebrini M, Lagrenée M, Vezin H, Traisnel M, Bentiss F (2007) Corros Sci 49:2254
24. Priya ARS, Muralidharam VS, Subramania A (2008) Corrosion 64:541
25. Bommersbach P, Alemany-Dumont C, Millet JP, Normand B (2006) Electrochim Acta 51:4011
26. Qu Q, Hao ZZ, Li L, Bai W, Liu YJ, Ding ZT (2009) Corros Sci 51:569
27. Lagrenée M, Mernari B, Bouanis M, Traisnel M, Bentiss F (2002) Corros Sci 44:573
28. Qu Q, Jiang SA, Li L, Bai W, Zhou J (2008) Corros Sci 50:35
29. Yang XM (1999) J Ningxia Univ 20:47 (in Chinese)
30. Schweinsberg DP, Ashworth V (1988) Corros Sci 28:539
31. Bentiss F, Traisnel M, Lagrenée M (2000) Corros Sci 42:127